

Synthetic aperture microscopy using off-axis illumination and polarization coding

Vicente Mico ^a, Zeev Zalevsky ^b, Javier García ^{c,*}

^a *AIDO, Technological Institute of Optics, Colour and Imaging, Cl. Nicolás Copérnico, 7-13 Parc Tecnològic 46980 Paterna, Valencia, Spain*

^b *School of Engineering, Bar-Ilan University, Ramat-Gan 52900, Israel*

^c *Departamento de Óptica, Universitat de València, Cl. Doctor Moliner, 50, 46100 Burjassot, Spain*

Received 10 November 2006; received in revised form 5 April 2007; accepted 20 April 2007

Abstract

A new method to improve the resolution of optical imaging systems beyond the classical Rayleigh resolution limit is presented. The technique relies on synthetic aperture generation in three stages. The first one (encoding stage) uses an illumination procedure that combines both on-axis and off-axis illumination beams with different polarization states onto the object. After the imaging system, a second stage (decoding stage) allows the recovering of the encoded spatial-frequency object information by means of an interferometric configuration based on the polarization coding carried out in the previous stage. Finally, a third stage (digital post-processing stage) is used to generate a synthetic aperture that is three times larger than the conventional aperture of the imaging system. The whole process allows us to obtain a superresolved image of the object. Experimental implementation of the approach for a commercial microscope objective is presented.

© 2007 Elsevier B.V. All rights reserved.

Keywords: Superresolution; Digital holography; Synthetic aperture microscopy; Fourier image formation

1. Introduction

The ability to improve the limited resolving power of optical imaging systems imposed by the wave nature of light has been widely studied throughout the years [1–20]. Due to the band limitation of imaging in terms of spatial frequencies, every optical system provides a limited spatial resolution that is defined by its numerical aperture (NA) and the illumination wavelength. Thus, the maximum lateral resolution that can be achieved by an optical system in air is $\lambda/2$ that corresponds with a NA equal to 1. Moreover, imaging systems with NA approaching unity are costly and not always practical (depending on the application). For this reason, many efforts have been made to improve the resolution without changing the physical prop-

erties of the optical imaging system: this is the aim of the superresolution techniques.

Great progress have been attained in superresolution methods applied to improve the resolution beyond the diffraction limit. Examples that overcome this limitation were given in near-field microscopy [1–4], stimulated emission depletion [5], structured illumination and patterned excitation [6–8], and saturable optical fluorescence microscopy [9–11].

Basically, the superresolution effect can be understood as a synthetic enlargement in the optical system aperture that improves the resolution of the optical system in comparison with the resolution presented by the same optical system without applying the superresolution approach. This task can be performed by an encoding–decoding process of the spatial-frequency object information that permits the passage of this additional information through the limited aperture of the imaging system. To understand this point, it is necessary to make use of the information

* Corresponding author. Tel.: +34 96 354 46 11; fax: +34 96 354 47 15.
E-mail address: javier.garcia.monreal@uv.es (J. García).

theory [12–14] that gives us an invariance theorem of the number of degrees of freedom of any optical system. After this invariance theorem, it is possible to improve the spatial bandwidth at the expense of another unused degree of freedom of the optical system, provided that some a priori information about the object is known. Some examples of this a priori information are that the object may be approximately time independent [15–17], polarization independent [18,19], mono-frequency (λ -independent) [20], or one dimensional [21]. The corresponding degree of freedom is thus used for enhancing spatial resolution.

Time multiplexing is a well-known approach used to obtain superresolution and can be implemented in a variety of ways [15–17,22]. The basic idea dates back to Françon [15] in 1952 and his idea is the root of today's confocal scanning microscopes. This temporal approach is based on synchronized moving pinholes, one over the object and another one in the image plane through an optical imaging system. Some years later, Lukosz [16] replaced the scanning pinholes by synchronized moving gratings, alleviating the low light efficiency problem and, therefore, reducing the long integration times of the Françon approach. The Lukosz approach had been accepted as the cornerstone of the time multiplexing superresolution and many modifications of the basic approach had been proposed over the years [22].

Another way to perform the Lukosz idea is thinking in terms of tilted beams. The key idea consists in observing the equivalence between a diffraction grating and a set of tilted beams (on-axis and off-axis beams) with the same propagation angles than those diffracted by the grating. Thus, in a similar way as in the Lukosz systems, the off-axis illumination is used to shift the high-frequency components of the object spectrum to low-frequency components in such a way that they can pass through the aperture of the system. After that, an interferometric recording is needed to shift back these transmitted object spectrum components toward their original location.

Bearing in mind this analogy, many methods [23–31] involving off-axis illumination, interferometric image plane recording and post-processing stage had been developed to achieve superresolution effect with temporally restricted objects in fields such as microscopy and lithography. Recently, Mico et al. [31] had implemented an approach in which a set of off-axis illumination beams impinges the object with the primary advantage that the full interferometric configuration is after the microscope lens. One of the interferometric arms is spatially filtered using a pinhole array in such a way that the DC of each tilted illumination beam is selected and they serve as the set of tilted reference beams. The method exhibits an improvement factor in resolution close to three with coherent illumination as well as a reduction in the sensitivity of the system to vibrations and/or thermal changes. But the gain in resolution is subordinated to the transmission of the zero frequency of the object spectrum by the microscope lens, that is, it is a function of the specific optical design of the microscope lens

that has been used. The present paper generalizes the approach shown in Ref. [31] with resolution improvement that is not limited by the specific microscope lens design.

The paper is organized as follows: Sections 2 and 3 give preliminary and theoretical analyses of the experimental setup, respectively. In Section 4 experimental results and the reconstruction process are presented. Section 5 concludes the paper.

2. Experimental configuration

The method presented here involves the generation of a synthetic enlargement in the aperture of a microscope lens that is achieved by means of three stages. In the following, some explanations about these three stages are described in detail.

The first stage is related with the illumination distribution produced onto the object, the *encoding stage*. A sketch of the encoding stage is depicted in Fig. 1. A non-polarized laser beam is directed onto a first one-dimensional (1D) diffraction grating. The 1D grating splits by diffraction the incoming beam in n different beams according to the diffraction angles specified in the grating equation, which is a function of the grating period and the illumination wavelength. For simplicity, we assume that the first 1D diffraction grating has three diffraction orders (0 and ± 1 orders). This assumption is realistic taking into account the large angles of the diffracted beams that will be used (as will be shown in the experiments). Owing to this separation it is simple to block the undesired orders. The three laser beams are directed towards the object. Without any other

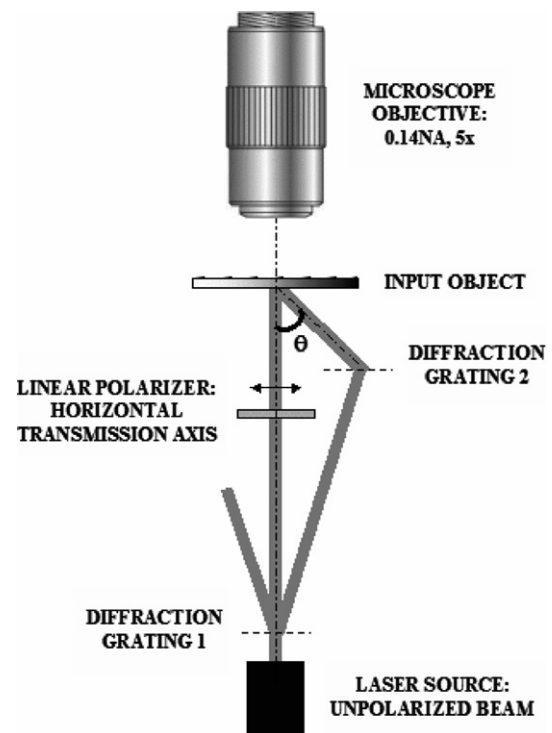


Fig. 1. Illumination system (encoding stage).

element, only the zero order would reach the object in the imaging region of interest. But due to the reason that the second 1D grating has a lower basic period and is placed at off-axis position, a second tilted laser beam can impinge the object by properly adjusting the axial position of both 1D diffraction gratings according to their diffraction angles.

To complete the encoding stage, a linear polarizer is introduced to define a horizontal polarization state of the on-axis illumination (zero order beam of the 1D first diffraction grating). This fact is represented by means of a horizontal arrow in Fig. 1. The significance of this polarizer will be understood in the decoding stage (Fig. 3). With this configuration, two beams illuminate the object region of interest simultaneously: the on-axis illumination beam with horizontal polarization state, and the off-axis non-polarized illumination beam with a θ tilt angle with respect to the on-axis beam. Assuming that the grating periods are significantly larger than the wavelength (condition that will be fulfilled in our experiments), the polarization does not play a significant role in the diffraction by the gratings.

By properly selecting the positions and the basic periods of both 1D gratings, the illumination angle θ of the off-axis beam can be adjusted to be twice the angle defined by the NA of the microscope lens. In this situation, a contiguous frequency band of the object spectrum passes through the limited aperture of the microscope lens. This effect is produced only in one dimension because the gratings are 1D and the configuration is static. For this reason, the resolution is near to be tripled only in one direction: the one defined by the off-axis illumination beam. To ensure off-axis illumination at the specific θ angle in a two-dimensional (2D) configuration, both 1D gratings are placed in rotatable holders which must be moved synchronously to ensure off-axis illumination onto the object. The previous procedure must be repeated for each frequency band that we want to obtain.

An off-axis illumination angle θ twice the one defined by the NA of the microscope lens enables to triple the resolution. This implies that a contiguous frequency band of the

object spectrum passes through the limited aperture of the microscope lens. This is shown in Fig. 2, where the coherent transfer function (CTF) of the imaging system is represented with a grey rectangular slot (Fig. 2a) and with a grey circle (Fig. 2b) for 1D and 2D cases, respectively. Naming $\Delta\nu$ the cut-off frequency of the imaging system, we must illuminate the object with an off-axis beam in order to downshift the contiguous frequency band inside the limited system aperture and ensure its transmission through it. This condition is completely fulfilled when the off-axis illumination beam has a carrier frequency f_{off} equal to $f_{\text{off}} = 2\Delta\nu$, or in other words $f_{\text{off}} = \frac{\sin\theta}{\lambda} = 2\Delta\nu = 2\frac{\text{NA}}{\lambda}$ which means that $\theta = \arcsin(2\text{NA})$.

In a strict way, the off-axis illumination angle θ must not be equal to twice the angle defined by the NA but for low numerical apertures it means a good approximation. In our case (0.14 NA), the ideal off-axis illumination angle must be 16.1° but the real angle is approximately 16° . So, a quasi-contiguous frequency band is processed.

The second stage, called *decoding stage*, is depicted in Fig. 3 and it enables us to recover each one of the frequency bands that had been transmitted through the microscope lens aperture for each one of the off-axis illumination beams. The setup is based on a Mach–Zehnder interferometer [31] that provides the complex amplitude recording needed for the synthetic aperture system. Behind the microscope objective, a polarizing beam splitter (PBS) splits the imaging beam into two polarized beams. The reflected beam with vertical polarization state (represented by a dot in the right branch in Fig. 3) allows image formation of the object onto the CCD after reflection in mirror M1. We call this branch as *imaging arm*. In the transmitted beam with horizontal polarization state (represented by a horizontal arrow in the left branch in Fig. 3), some elements are introduced to perform optical image processing. This branch is called *reference arm*. In the following, we explain in detail the configuration of the reference arm in this new superresolution technique.

The PBS allows the transmission of light with horizontal polarization state, that is, the on-axis beam and part of the

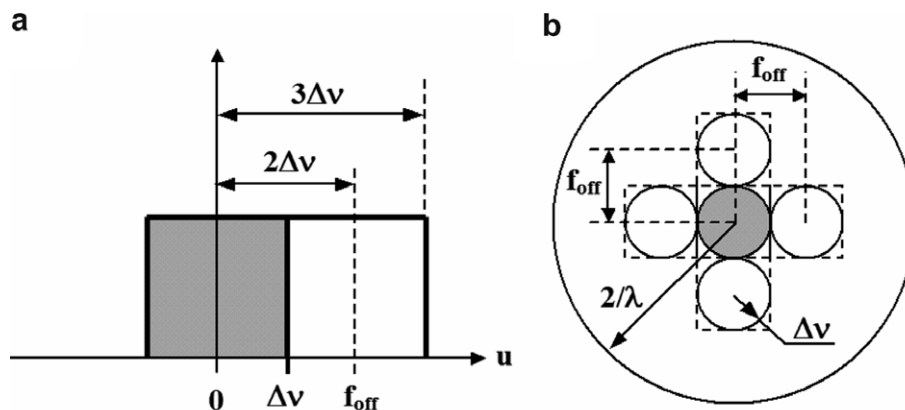


Fig. 2. Definition of the off-axis illumination angle to triple the cut-off frequency of the conventional imaging system: (a) 1D case with rectangular CTF, and (b) 2D case with circular CTF.

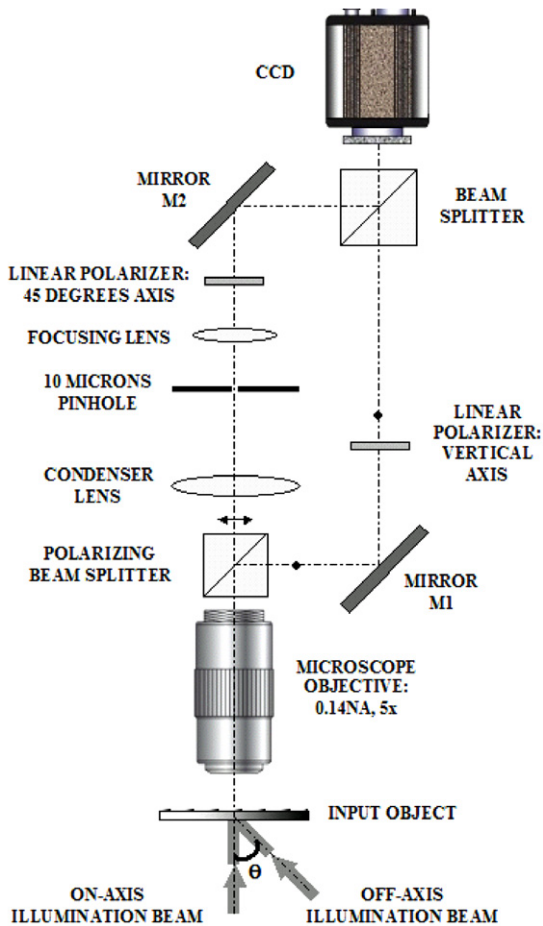


Fig. 3. Interferometric configuration (decoding stage).

off-axis beam, which is non-polarized. After the PBS, a first lens, called *condenser lens*, images the transmitted object spectrum that is composed by the addition of a central part (due to the on-axis beam) and a lateral frequency band (due to the off-axis beam). If a pinhole is placed at the center of this image plane, coinciding at the axial position of the central part of the object spectrum, only its DC term will be transmitted. This procedure gives a uniform reference beam by spatial filtering that can be used to perform the interferometric recording in the CCD plane. A second lens, called *focusing lens*, is introduced to compensate the curvature difference in the optical beams transmitted by both interferometric arms, allowing the holographic recording of the exact Fourier transform of the object. This lens could be avoided but a digital compensation of this spherical phase factor would be needed for each recorded hologram (see Ref. [26]).

At this point, two beams having orthogonal polarization states are directed towards the CCD by the action of a non-polarized beam splitter. To mix these polarization states in order to perform hologram recording, one can introduce a half wave plate at one of the interferometric arms provided that the optical wave plate axis is fixed to 45°. Instead of using the half wave plate, we use a linear polarizer placed in the reference arm the transmission axis of which forms

45° with the horizontal polarization state of the reference beam. Notice that by a slight rotation of the transmission axis, this polarizer helps us to maximize the visibility of the fringe pattern recorded at the CCD. Additionally, another linear polarizer with vertical transmission axis is placed in the imaging arm to increase the vertical polarization degree of the imaging beam after reflection at the BPS. Thus, by tilting the mirror M2, an off-axis digital hologram of the transmitted frequency band due to the off-axis illumination can be recorded. Repeating this process in sequential mode for different positions of the 1D gratings in the encoding stage enables us to recover each frequency band transmitted by the microscope lens provided that the tilt introduced is large enough to move aside the first diffraction order from the zero order in the hologram. Notice that no changes are introduced in the on-axis beam for the different off-axis recordings, so the reference beam is always present over the CCD to allow the holographic recording.

With this procedure, a set of quasi-contiguous frequency bands that implies additional information about the high-frequency content of the object can be sequentially recovered. To perform recording of the on-axis transmitted frequency band (central part of the object spectrum), only the on-axis illumination beam is sent onto the object. Then, the recovering of the central frequency band is performed by slightly rotating the first polarizer placed in front of the object in order to produce imaging and reference beams with the same frequency band in the decoding stage. This procedure cannot be made for the off-axis illumination cases because the intensity of the transmitted frequency band is not enough to synthesize reference beam using spatial filtering.

After the overall recording process is completed, a *digital post-processing stage* is needed. This third stage involves an inverse Fourier transformation of each of the recorded hologram, and a filtering and centering process of each one of the first diffraction hologram order to its proper

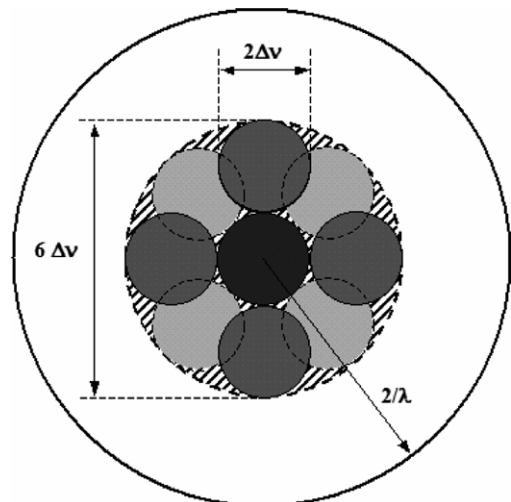


Fig. 4. Synthetic aperture generation (digital post-processing stage).

position in the original object spectrum. This results in the generation of a synthetic aperture as depicted in Fig. 4. Finally a direct Fourier transformation of the previous centered spectrum outputs the superresolved image.

Note that the use of a given grating frequency with different angles provides band-passes that are equally separated from the zero frequency spot. This arrangement of elementary pupils to build the synthetic aperture is not the only one. A different number of band-passes can be obtained at the expense of a higher number of exposures, and thus, total exposure time. A further increase of resolution would need a second grating with a higher period to cover a second outer ring in the frequency space.

3. System analysis

Let us now focus on the mathematical foundation using diffraction analysis of the experimental setup presented in Figs. 1 and 3. For the sake of simplicity, some implicit considerations about the experimental setup will be assumed.

The central band-pass can be recorded by slightly rotating the encoding polarizer. This action permits the passage of light through both arms in the decoding stage. When off-axis illumination is used, the imaging arm of the interferometric decoding stage provides the band-pass image of the object. Then, in both cases and under Fresnel approximation, the amplitude distribution at the image plane incoming from the imaging arm of the interferometric system is a scaled version of the input object, which is multiplied by the corresponding collimated beam and convolved with the point spread function (PSF) of the imaging system

$$U_{\text{CCD}}^{\text{Im}}(x, y) = \left\{ \left[f\left(-\frac{x}{M}, -\frac{y}{M}\right) e^{j2\pi(v_m x + v_n y)} \right] \otimes \text{disk}(\Delta v r) \right\} e^{j\frac{k}{2z'}(x^2 + y^2)} \quad (1)$$

where (x, y) are the spatial coordinates at the output plane, M is the image magnification, (v_m, v_n) the carrier frequency of the used illumination beam in the (X, Y) axis, and $k = 2\pi/\lambda$ the wave number. We will assume that the coherent transfer function of the system is a circular aperture with radius Δv , that is, $\text{circ}(\rho/\Delta v)$, and ρ is the radius in the spatial frequency domain. Thus, the PSF is its inverse Fourier transformation that we will denote as $\text{disk}(\Delta v \cdot r)$, where r is the radial coordinate in the output plane defined as $r = \sqrt{x^2 + y^2}$. Although the illumination used in the presented approach is collimated, a phase factor coming from the change in convergence introduced by the microscope lens is introduced in the image (last term in Eq. (1)). The distance z' is the distance between the axial point at the focal image plane of the microscope lens and the axial point at the image plane.

Let us now evaluate now the amplitude distribution incoming onto the CCD from the reference arm. Because of both the polarization coding and the on-axis illumination, the intensity of the transmitted beam in the PBS is high enough to perform a spatial filtering process. The condenser lens performs the image of the amplitude distribu-

tion formed in the image focal plane of the microscope lens, allowing us to place a pinhole in this image plane to extract the DC term. Thus, the amplitude distribution incoming from the reference arm can be summarized by an on-axis delta function at the pinhole plane. This point source emits a divergent illumination beam that is modified in divergence by the focusing lens (see Fig. 3). By means of an experimental adjustment of the axial position of the focusing lens, the image of the pinhole can be axially shifted up to the image focal plane of the microscope lens. Then, the divergence of both interferometric beams is made equal and the holographic recording will exhibit no spherical component in its carrier. In conclusion, the amplitude distribution incoming from the reference arm is proportional to

$$U_{\text{CCD}}^{\text{Ref}}(x, y) = e^{j\frac{k}{2z'}[x^2 + y^2] + j2\pi Qx} \quad (2)$$

where an additional linear phase factor, $\exp\{j2\pi Qx\}$, playing the role of a carrier with frequency Q is introduced by tilting the mirror M2. Note that we assume that the focusing lens does not trim the reference beam.

Thus, the overall amplitude that impinges on the CCD comes from the addition of Eqs. (1) and (2), and it gives the following intensity distribution that can be separated in four terms named as $T_1(x, y)$, $T_2(x, y)$, $T_3(x, y)$ and $T_4(x, y)$, respectively

$$\begin{aligned} I_{\text{CCD}}(x, y) &= |U_{\text{CCD}}^{\text{Im}}(x, y) + U_{\text{CCD}}^{\text{Ref}}(x, y)|^2 \\ &= 1 + |U_{\text{CCD}}^{\text{Im}}(x, y)|^2 + U_{\text{CCD}}^{\text{Im}}(x, y)[U_{\text{CCD}}^{\text{Ref}}(x, y)]^* \\ &\quad + [U_{\text{CCD}}^{\text{Im}}(x, y)]^* U_{\text{CCD}}^{\text{Ref}}(x, y) \\ &= T_1(x, y) + T_2(x, y) + T_3(x, y) + T_4(x, y) \end{aligned} \quad (3)$$

Eq. (3) represents the hologram recorded on the CCD for each one of the illumination codings produced onto the object. In the reconstruction procedure, we perform digitally an inverse Fourier transformation of Eq. (3) to analyse each term separately. We name (u, v) as the spatial frequencies in 1/pixels units corresponding to a digital Fourier transformation. The first term, $T_1(x, y) = 1$, is constant and its Fourier transform, $[\tilde{T}_1(u, v)]$ is just a delta function centred at the origin. The second term, $T_2(x, y)$, is the intensity of the recorded image. Thus, its Fourier transform $[\tilde{T}_2(u, v)]$, is also centred at the origin, with a width that doubles the original band-pass of the system.

The third and fourth terms in Eq. (3) contain the information about the phase and the amplitude of the object. The third term is

$$\begin{aligned} T_3(x, y) &= \left\{ \left[f\left(-\frac{x}{M}, -\frac{y}{M}\right) e^{j2\pi(v_m x + v_n y)} \right] \otimes \text{disk}(\Delta v r) \right\} \\ &\quad \times e^{j\frac{k}{2z'}[x^2 + y^2]} e^{-j\frac{k}{2z'}[x^2 + y^2]} e^{-j2\pi Qx} \end{aligned} \quad (4)$$

The Fourier transform of the third term, $[\tilde{T}_3(u, v)]$, represents a band-pass of the object spectrum shifted by the carrier frequency Q and placed at the left position of the central autocorrelation term (-1 diffraction order for the holographic recording process)

$$\tilde{T}_3(u, v) = K \left\{ [\tilde{f}(Mu, Mv) \otimes \delta(u - v_m, v - v_n)] \cdot \text{circ}\left(\frac{\rho}{\Delta v}\right) \right\} \otimes \delta(u + Q, v) \quad (5)$$

where K is a constant which also includes constant phase factors, and \tilde{f} is the Fourier transform of the input. Note that the fourth term in Eq. (4) is the complex conjugate of the third term and has a similar meaning. The last delta function in Eq. (5) implies a frequency shift in the transmitted spectral band-pass necessary to guarantee the separation between the -1 diffraction order from the zero order of the recorded hologram and can be controlled by tilting the mirror M2 in the reference arm.

Eq. (5) describes the information of the spectral frequency band-pass of the object spectrum transmitted by the microscope objective for a certain illumination beam defined by (v_m, v_n) . It must be located far enough from the zero order of the recorded hologram to avoid overlapping with the zero order term. Taking into account that the first order is $2\Delta v$ wide and the zero order is $4\Delta v$, a separation of $3\Delta v$ suffices. In the image domain this corresponds to a carrier frequency with period smaller than three times the plain image resolution spot size. On the other hand, the maximum separation is given by the Nyquist sampling rate so that the carrier frequency should be such that its period of the interferogram is larger than two pixels.

The term in square brackets in Eq. (5) implies a shift in the object spectrum according to the illumination beam used in the encoding stage. In other words, this is equivalent to produce the shift not in the object spectrum but in the circular aperture. Thus, Eq. (5) can be rewritten as

$$\tilde{T}_3(u, v) = K \left\{ \tilde{f}(Mu, Mv) \left[\text{circ}\left(\frac{\rho}{\Delta v}\right) \otimes \delta(u - v_m, v - v_n) \right] \right\} \otimes \delta(u + Q, v) \quad (6)$$

Eq. (6) allows us to identify the synthetic aperture as the expression in square brackets, obtained by sequentially recording the different holograms by repositioning the 1D diffraction gratings at the encoding stage

$$\text{SA}(u, v) = \text{circ}\left(\frac{\rho}{\Delta v}\right) \otimes \left[\sum_{m,n=1}^N \delta(u - v_m, v - v_n) \right] \quad (7)$$

In the presented approach, we perform eight off-axis illuminations recordings, aside the on-axis one, yielding an octagonal shape synthetic aperture (see Fig. 4). The size of the smallest circles corresponds to the NA of the microscope objective (Δv radius). The desired synthetic pupil (dashed circle line of $6\Delta v$ diameter approximately) is almost covered by the set of elemental apertures. The on-axis illumination pupil (dark gray in Fig. 4) is complemented with eight additional shifted apertures, all of them quasi-contiguous to the on-axis one. Four of them are accomplished by off-axis illuminations in (X, Y) orthogonal directions (medium gray level in Fig. 4). The other four pupils are obtained by off-axis illuminations for each oblique direction (light gray level in Fig. 4). The actual cut-off frequency is increased to three times the conven-

tional cut-off frequency of the microscope objective resulting in a notable resolution enhancement when an inverse Fourier transformation is produced to recover the superresolved object.

One important advantage of this superresolution approach is that the system transmits both interferometric beams through the microscope lens without penalty in the field of view and the system becomes robust because the holographic interferometric recording setup is done after the microscope lens. Moreover, the system ensures the transmission of the reference beam (on-axis illumination) for every off-axis beam used in the illumination procedure with independence of the specific optical design of the microscope lens. Further advantages are related to the possibility to work not only for real valued objects but also for complex or phase ones. Note that no assumption about the properties of the amplitude object $f(x, y)$ is made, so for any complex input distribution the reconstruction of the input may be obtained.

4. Experimental results

For the new proposed superresolution method we have used a laser source (532 nm wavelength) as illumination. We have used a long working distance Mitutoyo infinity corrected microscope objective with 0.14 NA and $5\times$ magnification. The collimated laser beam emitted by the laser source is directly directed towards the first 1D grating, which has a period $12.5 \mu\text{m}$ (80 lp/mm basic frequency) and is placed on a rotatable platform with its rotation axis aligned with the optical system axis. The zero and $+1$ first diffraction order are used as illumination beams onto the object. The zero order beam impinges directly the object after passing through a linear polarizer with horizontal transmission axis and the $+1$ diffraction order is used to perform off-axis illumination onto the object.

At the appropriate distance, a second 1D diffraction grating is placed onto another rotatable platform to allow off-axis illumination onto the object. The period of the second grating is $1.7 \mu\text{m}$ approximately (600 lp/mm basic frequency) and the illumination angle with respect to the on-axis beam (angle θ in Figs. 1 and 3) is 16° approximately. This tilted illumination beam ensures that a quasi-contiguous frequency band of the object spectrum will be transmitted through the microscope lens aperture. Note that 16° implies an illumination angle that is near to double the angle defined by the NA of the microscope lens ($\text{NA} = 0.14 \Rightarrow \theta' = 8.05^\circ$). Thus, by positioning in sequence the rotatable platforms of both 1D diffraction gratings in a set of eight different positions with 45° angular separation between consecutive positions, we will cover the full 2D space of the available off-axis illumination beams onto the object.

After the microscope lens, a polarizing beam splitter allows us to separate the imaging beam from the reference beam. The reference beam is condensed over a pinhole by a lens with 100 mm focal length. The pinhole has a diameter

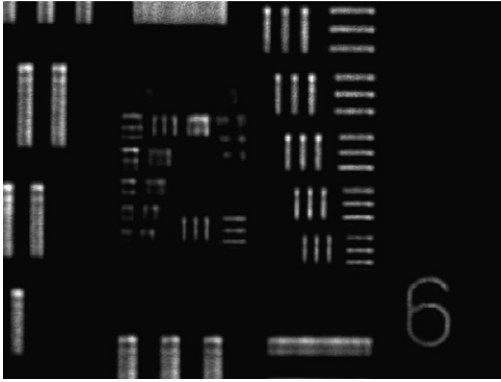


Fig. 5. Low resolution quality image.

of 10 μm . After the pinhole, a second lens with 80 mm focal length is placed to compensate the divergence difference between both interfering beams. Due to the horizontal polarization state of the reference beam, a linear polarizer with 45° transmission axis is placed after the focusing lens. The imaging beam is vertically polarized due to the reflection in the BPS and it is directed towards the CCD after reflection in mirror M2 and after passing through a linear polarizer with vertical transmission axis. This vertical polarizer ensures the complete extinction of the reference beam because the PBS does not extinguish completely the horizontal polarization state of the reference beam.

The on-axis frequency band recording is obtained by providing only on-axis illumination onto the object and

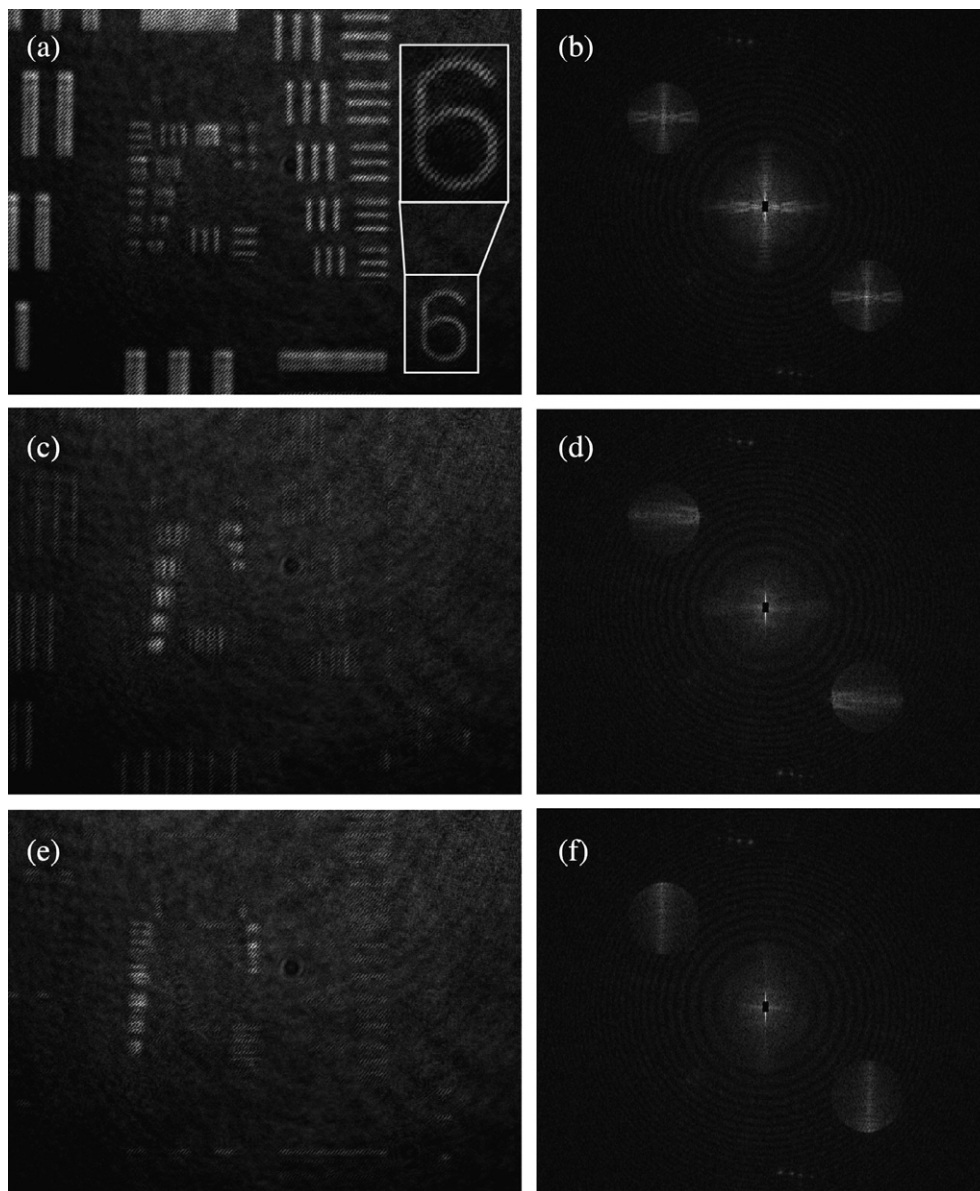


Fig. 6. Different off-axis recorded holograms and its Fourier transformation: on-axis illumination beam ((a) and (b)), off-axis horizontal illumination ((c) and (d)), and off-axis vertical illumination ((e) and (f)). The inset included in (a) case shows a magnified portion of the image where the interferometric fringes can be observed.

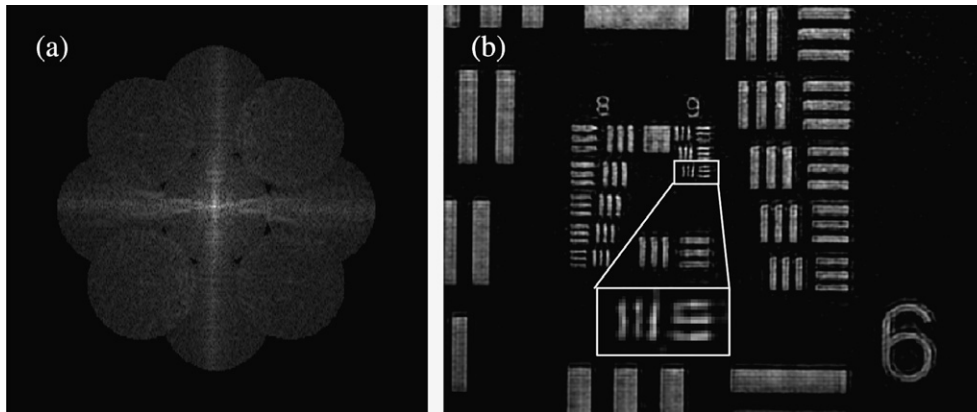


Fig. 7. Generated synthetic aperture (a) and superresolved image (b).

by slightly rotating of the transmission axis of the linear polarizer placed in the zero order of the first 1D grating. In addition to the on-axis illumination we have carried out eight off-axis illuminations in sequential mode to generate an octagonal synthetic aperture as depicted in Fig. 4. This particular arrangement and number of off-axis illuminations was chosen as a tradeoff between total image capture time (proportional to the number of exposures) and the coverage of the frequency space. A smaller number would result in significant uncovered regions in the spectrum. Less exposures could be made starting with a smaller angle for the off-axis illuminations (larger overlapping of the elementary pupils), but at the expense of a smaller resolution enhancement. The exposure time for each of the holograms is about 15 ms and the overall recording process can be done in a few seconds. The input object is a negative 1951 USAF high resolution test. Fig. 5 shows a low resolution image of the test target obtained with the 0.14 NA objective. Clearly, many spatial frequencies are not transferred by the low NA objective and a low pass version of the object test is obtained. The resolution spot size of the microscope lens is $1.74\ \mu\text{m}$ when coherent illumination is used, which corresponds to “Group 8, Element 2” resolution in the test target.

Then, we perform the superresolving approach using the recording of nine off-axis holograms. Fig. 6 shows the hologram for the on-axis illumination and its Fourier transformation, and two holograms and their Fourier transforms corresponding to the off-axis illumination exposures along the X and Y directions. The holograms have a noticeable coherent noise due to dust, multiple reflections, and diffraction patterns coming from the borders of the elements (off-the-shelf equipment). This can be greatly reduced in a real application by the use of a closed dust-free enclosure and elements specifically matched for the application in size and antireflection coating. After the nine off-axis holograms are recorded and stored in the computer memory, each of the frequency bands of the -1 hologram diffraction order is shifted to its correct position in the spectrum. Then, all of them are superimposed to synthesize the desired synthetic aperture. An inverse Fourier transform

yields the final superresolved image. Fig. 7 shows the generated octagonal synthetic aperture and the superresolved image, showing an improvement in resolution close to three for every object direction. As a consequence, the resolution spot size is reduced until $0.58\ \mu\text{m}$, which enable us to resolve the finest detail given by “Group 9, Element 3” of the Resolution Test Target ($645\ \text{lp/mm}$ cutoff frequency, $0.775\ \mu\text{m}$ resolution limit). So, the resolution improvement implies a synthetic aperture of approximately 0.45 SNA (Synthetic Numerical Aperture). As previously commented, the image is affected by some coherent noise, due to system imperfections and the typical ringing due to coherent imaging with sharp edge pupils is also visible. These artifacts do not impede to observe a close to three-fold resolution improvement.

Although the microscope magnification is $5\times$, we have introduced a higher magnification ($26\times$ approximately) in order to avoid aliasing problems in the recording process at the CCD. Thus, no geometrical limitations are presented in the resolution limit and only diffraction is degrading the final quality image. Exactly, the smallest period of the USAF resolution test is $1.55\ \mu\text{m}$ (Group 9, Element 3) and we use six pixels of the CCD camera to image this finest structure. So, we are above the Nyquist limit.

5. Conclusions

In this paper, we have described a superresolving approach for digital holographic microscopy where the superresolution effect is described in terms of a synthetic aperture generation. The synthetic aperture is generated by means of different frequency bands of the object spectrum that are sequentially obtained using off-axis illumination and polarization coding produced in an initial encoding stage that serves to illuminate the object. Recovery of each individual frequency band is possible using an optical decoding stage in interferometric configuration after the microscope lens that allows holographic recording process for each transmitted frequency band. A final relocation process of each frequency band to its original position in the object spectrum is produced in a third post-processing dig-

ital stage. From an implementation point of view, the method requires a separate exposure with rotation of the illumination system for every elementary pupil that will compose the synthetic aperture. With our standard mechanical equipment, this fact adds a bias time of less than one second to the global exposure time, and could be reduced with a specific equipment. The processing for each exposure (Fourier transform, relocation of the proper diffraction order and addition) does not add any significant time overhead to the implementation and can be performed in a regular computer. An improvement resolution factor of three is achieved, in comparison with the resolution of the tested microscope objective for a standard configuration.

One of the main advantages of the presented method is that the transmission of the imaging and reference beam is produced without reduction in the field of view of the microscope lens due to the encoding–decoding stage. On the other hand, the resolution improvement achieved in the presented approach is not dependant on the microscope objective optical design and the zero order (responsible for the reference beam in the interferometric setup) is always transmitted. Thus, a gain factor of three in resolution can be achieved for every microscope objective that has low and medium NA if the 1D diffraction gratings of the encoding stage are adjusted to produce the required illumination angle onto the object. The use of off-axis beams happens only prior to the sample (not inside the microscope interferometer itself). Thus, the system does not suffer the vignetting problems of other systems. The illumination system is based only on diffraction rulers and thus, vignetting can also be eliminated on this stage. Moreover, the system, as compared to previous setups, is simple and robust because the interferometric system is placed after the imaging lens and the whole recording process is done on the image space.

Acknowledgements

This work was supported by FEDER funds and the Spanish Ministerio de Educación y Ciencia under the Project FIS 2004-06947-C02-01.

References

- [1] D. Courjon, Near-Field Microscopy and Near-Field Optics, Imperial College Press, London, 2003.
- [2] E. Betzig, J.K. Trautman, T.D. Harris, J.S. Weiner, R.L. Kostelak, Proc. Natl. Acad. Sci. USA 251 (5000) (1991) 1468.
- [3] E. Betzig, J.K. Trautman, Proc. Natl. Acad. Sci. USA 257 (5067) (1992) 189.
- [4] E. Betzig, J.K. Trautman, J.S. Weiner, T.D. Harris, R. Wolfe, Appl. Opt. 13 (1992) 4563.
- [5] K.I. Willig, S.O. Rizzoli, V. Westphal, R. Jahn, S.W. Hell, Nature 440 (2006) 935.
- [6] M.G.L. Gustafsson, J. Microsc. 198 (2000) 82.
- [7] B. Littleton, K. Lai, D. Longstaff, V. Sarafis, P. Munroe, N. Heckenberg, H. Rubinsztein-Dunlop, Micron 38 (2007) 150.
- [8] R. Heintzmann, P.A. Benedetti, Appl. Opt. 45 (2006) 5037.
- [9] M.G.L. Gustafsson, Proc. Natl. Acad. Sci. USA 102 (2005) 13081.
- [10] M. Hofmann, Ch. Eggeling, S. Jakobs, S.W. Hell, Proc. Natl. Acad. Sci. USA 102 (2005) 17565.
- [11] R. Heintzmann, T.M. Jovin, C. Cremer, J. Opt. Soc. Am. A 19 (2002) 1599.
- [12] G. Toraldo di Francia, J. Opt. Soc. Am. 45 (1955) 497.
- [13] G. Toraldo di Francia, J. Opt. Soc. Am. 59 (1969) 799.
- [14] I.J. Cox, J.R. Sheppard, J. Opt. Soc. Am. A 3 (1986) 1152.
- [15] M. Françon, Il Nuovo Cimento (Suppl. 9) (1952) 283.
- [16] W. Lukosz, J. Opt. Soc. Am. 57 (1967) 932.
- [17] A. Shemer, D. Mendlovic, Z. Zalevsky, J. García, P. García-Martínez, Appl. Opt. 38 (1999) 7245.
- [18] A.W. Lohmann, D.P. Paris, Appl. Opt. 3 (1964) 1037.
- [19] A. Zlotnik, Z. Zalevsky, E. Marom, Appl. Opt. 44 (2005) 3705.
- [20] A.I. Kartashev, Opt. Spectra. 9 (1960) 204.
- [21] M.A. Grimm, A.W. Lohmann, J. Opt. Soc. Am. 56 (1966) 1151.
- [22] Z. Zalevsky, D. Mendlovic, Optical Super Resolution, Springer, 2002.
- [23] X. Chen, S.R. J. Brueck, Opt. Lett. 24 (1999) 124.
- [24] C.J. Schwarz, Y. Kuznetsova, S.R.J. Brueck, Opt. Lett. 28 (2003) 1424.
- [25] V. Mico, Z. Zalevsky, P. García-Martínez, J. García, Opt. Exp. 12 (2004) 2589.
- [26] V. Mico, Z. Zalevsky, P. García-Martínez, J. García, Appl. Opt. 45 (2006) 822.
- [27] E.N. Leith, D. Angell, C.-P. Kuei, J. Opt. Soc. Am. A 4 (1987) 1050.
- [28] E.N. Leith, Opt. Lett. 15 (1990) 885.
- [29] V. Mico, Z. Zalevsky, J. García, Opt. Exp. 14 (2006) 5168.
- [30] M.G.L. Gustafsson, J. Microsc. 198 (2000) 82.
- [31] V. Mico, Z. Zalevsky, P. García-Martínez, J. García, J. Opt. Soc. Am. A 23 (2006) 3162.